

## Boundary-Layer Disruption and Heat-Transfer Enhancement in Convection Turbulence by Oscillating Deformations of Boundary

Leiqi Yuan<sup>1</sup>, Shufan Zou<sup>2</sup>, Yantao Yang<sup>1,3,\*</sup> and Shiyi Chen<sup>4,5,1,†</sup>


<sup>1</sup>State Key Laboratory for Turbulence and Complex Systems, and Department of Mechanics and Engineering Science, College of Engineering, Peking University, Beijing 100871, People's Republic of China

<sup>2</sup>College of Aerospace Science and Engineering, National University of Defense Technology, Changsha 410073, China

<sup>3</sup>Joint Laboratory of Marine Hydrodynamics and Ocean Engineering, Laoshan Laboratory, Shandong 266299, People's Republic of China

<sup>4</sup>Eastern Institute for Advanced Study, Eastern Institute of Technology, Ningbo, Zhejiang 315200, People's Republic of China

<sup>5</sup>Department of Mechanics and Aerospace Engineering, Southern University of Science and Technology, Shenzhen 518055, People's Republic of China

 (Received 26 July 2022; revised 31 March 2023; accepted 20 April 2023; published 18 May 2023)

In this Letter, we propose a novel strategy for significantly enhancing the heat transfer in convection turbulence. By introducing a boundary deformation of the standing-wave type, flow modulation can be realized when the amplitude is comparable or larger than the boundary-layer thickness. For a fixed moderate frequency, the entire fluid layer follows the boundary motion at small wave numbers, while only the near-wall regions are affected by the boundary deformation at large wave numbers. The heat-flux enhancement happens for the latter. For a fixed wave number and gradually increasing frequency, the vortical flows inside the wave valleys exhibit nonlinear transition and alter the distribution of boundary heat flux, and the global heat flux increases significantly at large enough frequencies. The current findings suggest that oscillating deformations of boundary can efficiently break the boundary layers, which serves as the bottleneck of global heat transfer, and open a new venue for modulating the convection turbulence.

DOI: [10.1103/PhysRevLett.130.204001](https://doi.org/10.1103/PhysRevLett.130.204001)

Turbulent convection controls the mixing and transport processes in many natural environments and engineering applications, such as geophysical flows and bioflows [1–3]. The canonical model for convection turbulence is the Rayleigh-Bénard convection (RBC), where the fluid between two horizontal plates is heated from below and cooled from above. The flow domain of the RBC can be spatially divided into the thin boundary-layer (BL) regions adjacent to the top and bottom plates and the bulk in between. Thermal plumes originated from BLs penetrate into the bulk and drive large-scale convection rolls there. The interplay among the BLs, the plumes, and the turbulent bulk is highly nonlinear and produces very rich dynamics, which makes the RBC one of the most classic paradigms in fluid mechanics [4–6].

Manipulating the coherent structures in the RBC attracts immense interest for two reasons. From a fundamental point of view, valuable insights about the nonlinear dynamics of turbulent flows can be obtained by intentionally modifying these coherent structures, such as the horizontal geometry confinement [7,8] and the asymmetric ratchet surfaces [9]. While from an application point of view, such manipulations often affect the global transport efficiency, which is highly desired in numerous engineering situations.

Various strategies have been proposed for coherent structure manipulation and to successfully enhance the

heat flux. For instance, the bulk region can be altered to a more transfer-efficient state by horizontal confinement [7,8], background rotation [10,11], second stabilizing scalar gradient [10,12], and vertical riblets or round solid obstacles [13–15]. Meanwhile, since the conductive BLs usually act as the bottleneck of heat transfer in the RBC, it is then very natural to disturb the BLs and achieve heat-transfer enhancement. Wall roughness has long been used to modify the RBC and increase the heat flux [16–20], for which one key rule is that the roughness should be high enough to penetrate the thermal BLs.

Another effective strategy is periodic modulations. It is well known that periodic forcing induces nontrivial behaviors in wall-bounded turbulence, such as pipe, channel, and Taylor-Couette flows [21–23]. In RBC, the horizontal vibration can strongly destabilize the thermal BL and promote the plume eruption, and the heat flux can be increased by up to 600% compared to the uncontrolled RBC [24]. When the periodic modulation is applied to the temperature of the bottom hot boundary, a Stokes thermal BL develops adjacent to the boundary and the global transport can be enhanced by about 25% for optimal parameters [25]. This strategy has been recently confirmed by experiments [26]. It should be noted, though, in the former work the angular frequency of vibration needs to be larger than 200 for observable enhancement [24]. Note that

the frequency is nondimensionalized by the free-fall time-scale  $\tau = \sqrt{H/(\alpha g \Delta)}$ , with  $H$  being the height of the fluid layer,  $\alpha$  as the thermal expansion coefficient,  $g$  as the gravitational acceleration, and  $\Delta$  as the temperature difference across the layer, respectively. While in the latter work, although the optimal frequency is of order  $10^{-2}$  for the maximal 25% of heat-flux increment, the amplitude of the periodic modulation is the same as the total temperature difference  $\Delta$ , saying a relatively large amplitude [25].

Here we propose a new modulation method to the turbulent convection flows. By introducing boundary deformation of the standing-wave type, the BL is mechanically disturbed and the heat flux can be enhanced significantly, saying over 100% increment compared to RBC. Moreover, this significant enhancement is achieved with the deformation amplitude of the order of BL thickness and at the moderate frequency. Therefore, the current Letter opens a new venue for flow modulation in thermal convection.

Consider a fluid layer bounded by two boundaries that deform according to the same standing-wave law,

$$z(x, y, t) = z_0 - A \cos(2\pi kx) \cos(2\pi ky) \cos(2\pi ft). \quad (1)$$

Here  $x$  and  $y$  are the horizontal coordinates,  $z$  is the vertical coordinate opposite to the gravity, and  $t$  is time, respectively.  $z_0 = 0$  ( $H$ ) is the neutral height when the bottom (top) boundary is flat.  $k$  is the wave number, which is the same in the two horizontal directions.  $A$  is the amplitude. Note the deformation has the same phase for the two boundaries, thus the actual height of the fluid layer always equals  $H$ . Both boundaries have constant temperatures with a difference  $\Delta$ . The governing equations under the Oberbeck-Boussinesq approximation are solved with our in-house code, which utilizes a second-order finite difference scheme and a fraction-time-step method for the incompressible flows [27]. The boundary deformation is implemented by a sharp-boundary type of immersed-boundary method [28]. Throughout this Letter, the same working fluid is used with the Prandtl number  $\text{Pr} = \nu/\kappa$  fixed at 1. The strength of the thermal driving is measured by the Rayleigh number  $\text{Ra} = (\alpha g \Delta H^3)/(\nu \kappa)$ , with  $\nu$  being the kinematic viscosity and  $\kappa$  the thermal diffusivity, respectively. Numerical simulations are conducted for various combinations of  $A$ ,  $k$ , and  $f$  over the range  $10^6 \leq \text{Ra} \leq 10^8$ , and details are summarized in the Supplemental Material [29].

*Effects of amplitude and wave number.*—We first fix the frequency at  $f\tau = 1$  and investigate five groups of cases with different combinations of  $(\text{Ra}, A/H)$ . For each combination the nondimensional wave number,  $kH$  is gradually increased from 0.5 to 8. The heat flux is measured by the nondimensional Nusselt number  $\text{Nu} = F_{\text{tot}}/(\kappa \Delta H^{-1})$ , with  $F_{\text{tot}}$  being the mean total flux measured over the horizontal plane at the midheight.

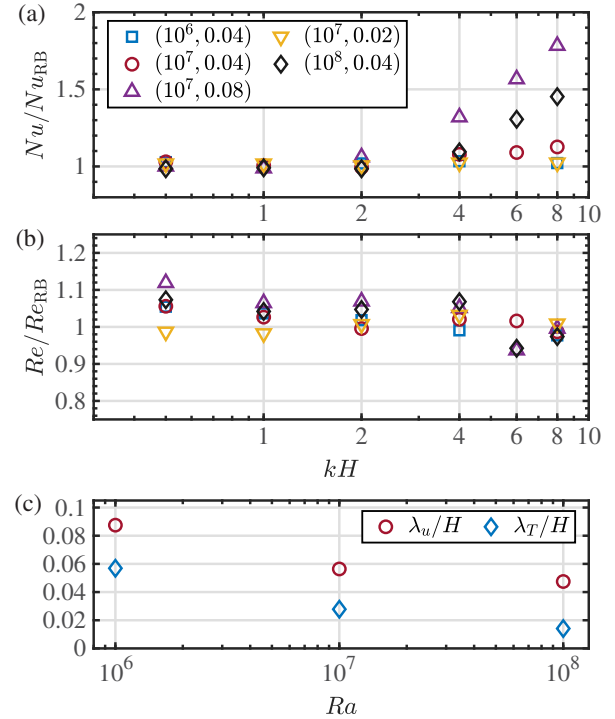


FIG. 1. (a) The Nusselt number ratio  $\text{Nu}/\text{Nu}_{\text{RB}}$  and (b) the Reynolds number ratio  $\text{Re}/\text{Re}_{\text{RB}}$  versus the wave number  $kH$ , respectively. In (a) and (b), different symbols represent different combinations of  $(\text{Ra}, A/H)$  as indicated in the legend of (a). (c) The viscous and thermal boundary-layer thicknesses versus the Rayleigh number for the RB flow.

The heat-flux enhancement is then measured by the ratio  $\text{Nu}/\text{Nu}_{\text{RB}}$ , with  $\text{Nu}_{\text{RB}}$  being the corresponding RBC with the same  $\text{Ra}$  number. The Reynolds number is defined as  $\text{Re} = u_{\text{rms}}H/\nu$ , with  $u_{\text{rms}}$  being the root-mean-square (rms) value of velocity magnitude calculated over the entire fluid domain. Similarly, the ratio  $\text{Re}/\text{Re}_{\text{RB}}$  is used to indicate the strengthening of flow motions. As shown by Figs. 1(a) and 1(b), which plot the two ratios versus the wave number, the heat-flux enhancement happens at large  $kH$  for  $(\text{Ra}, A/H) = (10^7, 0.04)$ ,  $(10^7, 0.08)$ , and  $(10^8, 0.04)$ . Meanwhile, for all cases, the Reynolds number does not change much compared to the RB cases, especially for the cases with heat-flux enhancement at large  $kH$ . Therefore, the heat-flux enhancement at large wave numbers is not accompanied by the strengthening of flow motions.

Actually, the appearance of heat-flux enhancement is highly related to the relative height of boundary deformation compared to the BL thickness of the uncontrolled RB flows. The viscous BL thickness  $\lambda_u$  and the thermal BL thickness  $\lambda_T$  are determined by the peak locations in the rms profiles of horizontal velocity and temperature of RB flows, respectively. Figure 1(c) displays  $\lambda_u$  and  $\lambda_T$  for the three Rayleigh numbers considered here. It is immediately clear that heat-flux enhancement at large  $kH$  only happens when  $A/H$  is larger than thermal BL thickness or both the viscous and thermal BL thicknesses. For the two groups

with  $(Ra, A/H) = (10^6, 0.04)$  and  $(10^7, 0.02)$ , the amplitude is smaller than both  $\lambda_u$  and  $\lambda_T$ , and no enhancement is obtained.

The above results indicate that for fixed  $f\tau = 1$  the observable heat-flux enhancement is achieved when the amplitude is larger than the thermal BL thickness and when the wave number is large enough. The difference between the large and small wave numbers is caused by different responses of the fluid layer to the boundary oscillation. As discussed in the Supplemental Material [29], from the perspective of thermal dissipation rate, the heat flux is highest when the boundary has the largest deformation. Therefore, in the following we focus on the flow fields at the maximal deformation phase. Figures 2(a) and 2(b) (and the corresponding video in the Supplemental Material) reveal that, for the small wave number  $kH = 0.5$ , the whole fluid layer follows the movement of boundaries, and the large-scale rolls in the bulk change the direction of circulations according to the boundary oscillation. For the large wave number  $kH = 8$ , the boundary deformation

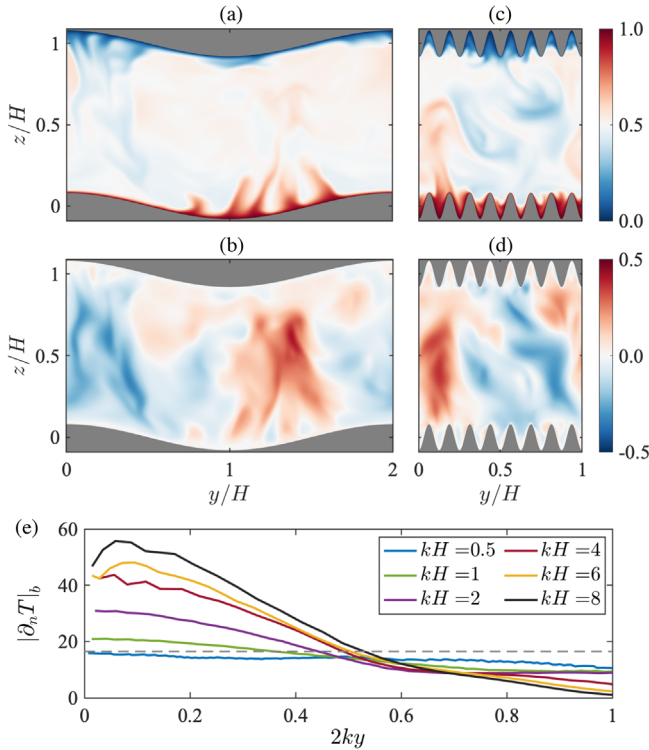


FIG. 2. Contours of (a),(c) temperature and (b),(d) vertical velocity on the vertical slice when the boundaries reach maximal deformation. Two cases are shown for  $Ra = 10^7$  and  $A/H = 0.08$ . (a),(b) is for the case with  $kH = 0.5$  and (c),(d) is for the case with  $kH = 8$ , respectively. (e) The temporal and phase averaged wall-normal temperature gradient  $|\partial_n T|_b$  over half wavelength at the lower boundary when the boundary reaches the maximal deformation.  $2ky = 0$  corresponds to wave crest and 1 to wave valley. Different curves are for different wave numbers at  $Ra = 10^7$ . The horizontal dashed gray line marks the value of RB flow.

only affects the adjacent regions and the bulk convection rolls are still driven by thermal plumes. Moreover, for the latter the wave crests penetrate into the bulk when the amplitude is larger than BL thickness, which causes the increase of boundary heat flux at the wave crests, as indicated by Fig. 2(e). The increment becomes larger as  $k$  increases. Meanwhile, for the lower boundary at the wave valleys, the boundary flux reduces due to the local accumulation of high temperature fluid, but this reduction is much weaker than the increase at the crests. Therefore, the overall heat flux is elevated for higher  $k$ .

*Effects of frequency.*—We now turn to the influence of changing frequency. The wave number is fixed at  $kH = 4$ , and three combinations of  $(Ra, A/H)$  are investigated with gradually increasing  $f$ . For these three groups, the amplitude  $A/H$  is larger than the thermal BL thickness of corresponding RB flows. The variations of  $Nu/Nu_{RB}$  and  $Re/Re_{RB}$  versus the nondimensional frequency  $f\tau$  are plotted in Figs. 3(a) and 3(b). Both ratios share very

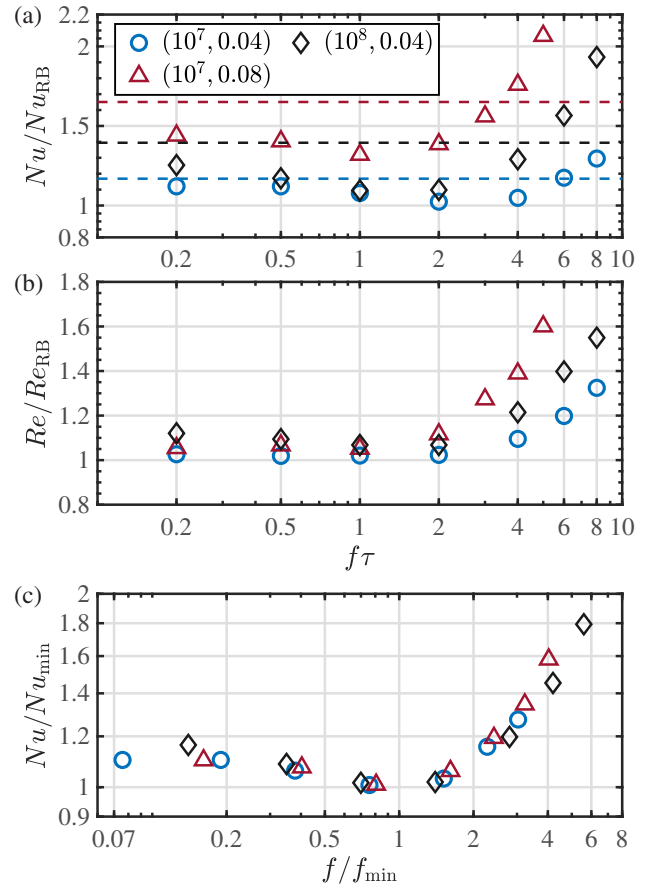


FIG. 3. (a) The Nusselt number ratio  $Nu/Nu_{RB}$  and (b) the Reynolds number ratio  $Re/Re_{RB}$  versus the frequency  $f\tau$  for fixed  $kH = 4$ , respectively. (c)  $Nu$  versus  $f$  with the two variables normalized by the minimum  $Nu_{min}$  and the corresponding frequency  $f_{min}$ . Different symbols represent different combinations of  $(Ra, A/H)$  as indicated in the legend of (c). The dashed lines in (a) indicate the value for  $f\tau = 0$ , with the line color the same as the symbols for the same  $(Ra, A/H)$ .

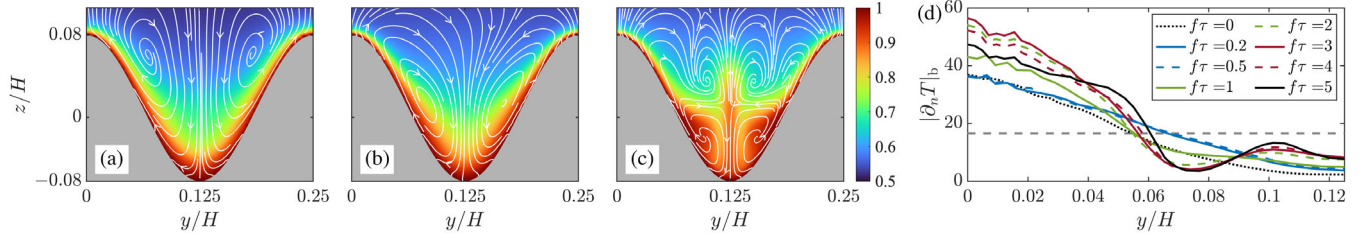


FIG. 4. (a)–(c) The contours of temperature fields overlaid by the streamlines on a vertical slice over one wave pattern for  $f\tau = 0.2, 1,$  and  $5$ , respectively. (d) The distributions of boundary temperature gradient over half wavelength for increasing  $f\tau$  with  $y/H = 0$  corresponding to the wave crest. For all panels, the quantities are calculated from the data on a vertical slice cutting the wave crest and averaged over time and different wave patterns for the phase with maximal boundary deformation. In (d) the horizontal dashed gray line marks the value of RB flow.

similar nonmonotonic variations among the three groups: They first slightly decrease and then rapidly increase as  $f\tau$  becomes larger. The highest heat-flux enhancement with respect to the RB flow can exceed 100% for  $(\text{Ra}, A/H) = (10^7, 0.08)$  and  $f\tau = 5$ . Unlike the situation of the increasing wave number, now the enhancement in heat transfer is accompanied by the increasing of  $\text{Re}$  or stronger flow motions. Furthermore, if one normalizes  $\text{Nu}$  by the respective minimum  $\text{Nu}_{\min}$  and the corresponding frequency  $f_{\min}$ , all three curves roughly collapse with each other, see Fig. 3(c). Here the minimum and its location are determined by the spline interpolation for each group of cases.

The nonmonotonic variation of  $\text{Nu}$  versus  $f$  is caused by the nonlinear response of flow structures to boundary deformation, which, in turn, modify the near-wall temperature distribution and the boundary heat flux. Figures 4(a)–4(c) show the temporal and phase averaged flow fields for three different frequencies when boundary deformation is maximal, and Fig. 4(d) plots the distribution of boundary heat flux for increasing frequency. The temporal evolution of these structures at different frequency can be seen more clearly in the videos in the Supplemental Material [29]. At  $f\tau = 0.2$ , two vortices are induced inside the wave valley and their centers are at the upper part of valley. Simulation shows that, for the stationary wavy boundary with the same wave number and amplitude, i.e.,  $f\tau = 0$ , the averaged flow field is very similar to that shown in Fig. 4(a) but with weaker mean currents. For the flow region shown in Fig. 4(a), the maximal velocity is about  $0.044U_f$  with  $U_f = H/\tau$  being the free-fall velocity. Whereas for  $f\tau = 0$  the same quantity is about  $0.032U_f$ . The surface heat-flux distributions indicate that for zero and low frequencies, the heat flux is the strongest and larger than the RB value at the crest, and the lowest and smaller than the RB value at the trough, respectively. Note the local mean flow is rather weak. The variation of surface heat flux is probably due to the different height. The wave crests penetrate into the bulk while the wave troughs are shielded by the local high temperature regions.

As  $f\tau$  increases, the two vortices move downward closer to the boundary and become stronger. For the flow region

shown in Fig. 4(b) with  $f\tau = 1$ , the local maximal velocity is about  $0.087U_f$ . With the changes in the vortices' location and strength, the heat flux increases at both the crest and trough. Moreover, the boundary heat flux beneath the vortices is smaller compared to the case with lower frequency, see the local minima around  $y/H = 0.07$  in Fig. 4(d). For even higher frequency, two pairs of vortices exist inside the wave valley. The local velocity maximum can be as high as  $0.5U_f$  for the flow field with  $f\tau = 5$  shown in Fig. 4(c). Now the boundary heat flux exhibits more complex distribution since it is affected by multiple vortices. Although the heat flux at crest is now smaller than those for intermediate frequencies, the heat flux around  $z/H = 0$  is higher. Because of the 3D geometry of boundary, smaller  $z$  corresponds to large surface area around each wave peak. Therefore, the total heat flux is still larger for higher frequency.

Since the boundary deformation with high frequency can strongly disrupt the original boundary layers that serve as the bottleneck of heat transfer in the RBC, the exponent  $\zeta$  in the scaling  $\text{Nu} \sim \text{Ra}^\zeta$  is considerably larger than the RB value, as illustrated by the compensated plot in Fig. 5 for fixed  $A/H = 0.04$ ,  $kH = 4$ , and  $f\tau = 8$ . For the RB flow, the linear fitting gives  $\zeta_{\text{RB}} = 0.3 \pm 0.03$ , which is consistent with existing studies [4]. However, for the flow with deforming boundary, the exponent  $\zeta$  gradually increases toward  $1/2$ , which is the value for the so-called ultimate regime. Similar behavior has also been found in RBC with horizontal vibration [24].

Two final remarks should be made. First, the surface area of boundary is larger than RBC when the deformation is introduced. Increasing of surface area does favor the heat-transfer rate, but it alone cannot account for all of the enhancement obtained here, especially for the regime with large  $f$ , as discussed in detail in the Supplemental Material [29]. Second, extra kinetic energy is ejected into the system by the boundary deformation. The minimal work required to generate the oscillation deformation is that to resist the pressure and viscous stress on the boundary. Calculation reveals that this energy is larger than the potential energy released by convection. However, the ratio between the two

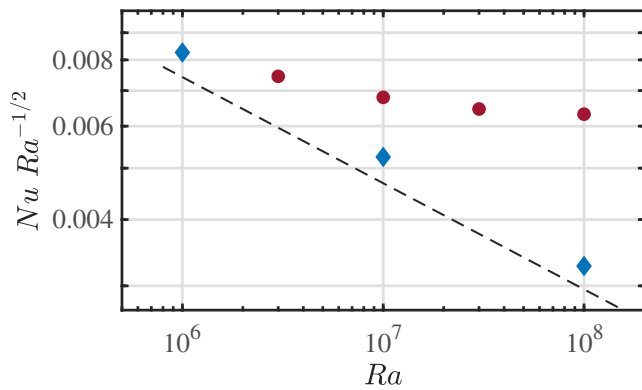


FIG. 5. The compensated plot of the Nusselt number versus the Rayleigh number for fixed  $A/H = 0.04$ ,  $kH = 4$ , and  $f\tau = 8$ , shown by the red circles. The blue diamonds mark the RB cases with flat boundary with the dashed line indicating the  $Nu \sim Ra^{0.3 \pm 0.03}$  scaling.

is smaller for larger  $Ra$  and smaller amplitude, see Fig. 4 of the Supplemental Material [29]. Therefore, one may anticipate that, for even larger  $Ra$ , as usually found in real applications, the ratio should be even smaller and may drop below unit.

**Conclusions.**—We demonstrate that the boundary deformation of the standing-wave type can efficiently alter the global responses of convection turbulence when the deforming amplitude is comparable to or larger than the BL thickness of RB flows. For small wave number, the whole fluid layer follows the movement of the boundaries. When the wave number is large enough, only flow regions close to boundary are disturbed. Local boundary heat flux is enhanced at wave crests and suppressed at wave troughs. For fixed intermediate frequency, the global heat flux increases as wave number and amplitude become larger, but the strength of flow motions does not change much.

The change of frequency has more profound influences on the flow morphology and global responses. As the frequency becomes higher, the vortical flows inside the wave valley show increasing strength and nonlinear transition of morphology, and the total heat-transfer enhancement increases with frequency. For fixed properties of standing wave, the exponent in the power-law scaling of the Nusselt number versus the Rayleigh number increases and approaches the value for the ultimate regime, as the mechanical perturbation can efficiently break the BLs that serve as the bottleneck of heat transfer.

The current results highlight the great potential of boundary deformation in flow modulations and open new venues for future investigations to fully exploit the proposed method. For instance, as  $Ra$  increases, the effective amplitude can be smaller as the BL thickness decreases. This implies that such heat-flux enhancement is easier to achieve at high  $Ra$ . The oscillating boundary deformation may be realized by microelectronic mechanical systems, and practical applications can be expected.

This work is financially supported by the National Nature Science Foundation of China under the Grant No. 11988102. Y. Y. also acknowledges the financial support from Laoshan Laboratory under the Grant No. LSKJ202202000.

\*yantao.yang@pku.edu.cn

†chensy@sustech.edu.cn

- [1] P. Charbonneau, Solar dynamo theory, *Annu. Rev. Astron. Astrophys.* **52**, 251 (2014).
- [2] M. Bees, Advances in bioconvection, *Annu. Rev. Fluid Mech.* **52**, 449 (2020).
- [3] C. Muller, D. Yang, G. Craig, T. Cronin, B. Fieldier, J. Haerter, C. Hohenegger, B. Mapes, D. Randall, S. Shamekh, and S. Sherwood, Spontaneous aggregation of convective storms, *Annu. Rev. Fluid Mech.* **54**, 133 (2022).
- [4] G. Ahlers, S. Grossmann, and D. Lohse, Heat transfer and large scale dynamics in turbulent Rayleigh-Bénard convection, *Rev. Mod. Phys.* **81**, 503 (2009).
- [5] D. Lohse and K.-Q. Xia, Small-scale properties of turbulent Rayleigh-Bénard convection, *Annu. Rev. Fluid Mech.* **42**, 335 (2010).
- [6] K.-Q. Xia, Current trends and future directions in turbulent thermal convection, *Theor. Appl. Mech. Lett.* **3**, 052001 (2013).
- [7] S. D. Huang, M. Kaczorowski, R. Ni, and K. Q. Xia, Confinement-Induced Heat-Transport Enhancement in Turbulent Thermal Convection, *Phys. Rev. Lett.* **111**, 104501 (2013).
- [8] K. L. Chong, S. D. Huang, M. Kaczorowski, and K. Q. Xia, Condensation of Coherent Structures in Turbulent Flows, *Phys. Rev. Lett.* **115**, 264503 (2015).
- [9] H. Jiang, X. Zhu, V. Mathai, R. Verzicco, D. Lohse, and C. Sun, Controlling Heat Transport and Flow Structures in Thermal Turbulence Using Ratchet Surfaces, *Phys. Rev. Lett.* **120**, 044501 (2018).
- [10] K. L. Chong, Y. Yang, S.-D. Huang, J.-Q. Zhong, R. J. A. M. Stevens, R. Verzicco, D. Lohse, and K.-Q. Xia, Confined Rayleigh-Bénard, Rotating Rayleigh-Bénard, and Double Diffusive Convection: A Unifying View on Turbulent Transport Enhancement through Coherent Structure Manipulation, *Phys. Rev. Lett.* **119**, 064501 (2017).
- [11] Y. Yang, R. Verzicco, D. Lohse, R. J. A. M. Stevens, D. Lohse, and K.-Q. Xia, What rotation rate maximizes heat transport in rotating Rayleigh-Bénard convection with Prandtl number larger than one?, *Phys. Rev. Fluids* **5**, 053501 (2020).
- [12] Y. Yang, R. Verzicco, and D. Lohse, From convection rolls to finger convection in double-diffusive turbulence, *Proc. Natl. Acad. Sci. U.S.A.* **113**, 69 (2016).
- [13] Y. Bao, J. Chen, B.-F. Liu, Z.-S. She, J. Zhang, and Q. Zhou, Enhanced heat transport in partitioned thermal convection, *J. Fluid Mech.* **784**, R5 (2015).
- [14] S. Liu, L. Jiang, K. L. Chong, X. Zhu, Z.-H. Wan, R. Verzicco, R. J. A. M. Stevens, D. Lohse, and C. Sun, From Rayleigh-Bénard convection to porous-media convection: How porosity affects heat transfer and flow structure, *J. Fluid Mech.* **895**, A18 (2020).

- [15] S. Liu and S. G. Huisman, Heat transfer enhancement in Rayleigh-Bénard convection using a single passive barrier, *Phys. Rev. Fluids* **5**, 123502 (2020).
- [16] Y.-C. Xie and K.-Q. Xia, Turbulent thermal convection over rough plates with varying roughness geometries, *J. Fluid Mech.* **825**, 573 (2017).
- [17] M. S. Emran and O. Shishkina, Natural convection in cylindrical containers with isothermal ring-shaped obstacles, *J. Fluid Mech.* **882**, A3 (2020).
- [18] X. Zhu, R. J. A. M. Stevens, R. Verzicco, and D. Lohse, Roughness-Facilitated Local  $1/2$  Scaling Does Not Imply the Onset of the Ultimate Regime of Thermal Convection, *Phys. Rev. Lett.* **119**, 154501 (2017).
- [19] X. Zhu, R. Stevens, O. Shishkina, R. Verzicco, and D. Lohse,  $Nu \sim Ra^{1/2}$  scaling enabled by multiscale wall roughness in Rayleigh-Bénard turbulence, *J. Fluid Mech.* **869**, R4 (2019).
- [20] G. Xu, Q. Wang, Z. Wan, and D. Sun, Heat transfer and plume statistics in turbulent thermal convection with sparse fractal roughness, *Journal of hydrodynamics* **33**, 1065 (2021).
- [21] C. Weng, S. Boij, and A. Hanifi, Numerical and theoretical investigation of pulsatile turbulent channel flows, *J. Fluid Mech.* **792**, 98 (2016).
- [22] T. O. Jelly, R. C. Chin, S. J. Illingworth, J. P. Monty, I. Marusic, and A. Ooi, A direct comparison of pulsatile and non-pulsatile rough-wall turbulent pipe flow, *J. Fluid Mech.* **895**, R3 (2020).
- [23] R. A. Verschoof, A. K. te Nijenhuis, S. G. Huisman, C. Sun, and D. Lohse, Periodically driven Taylor-Couette turbulence, *J. Fluid Mech.* **846**, 834 (2018).
- [24] B.-F. Wang, Q. Zhou, and C. Sun, Vibration-induced boundary-layer destabilization achieves massive heat-transport enhancement, *Sci. Adv.* **6**, eaaz8239 (2020).
- [25] R. Yang, K. L. Chong, Q. Wang, R. Verzicco, O. Shishkina, and D. Lohse, Periodically Modulated Thermal Convection, *Phys. Rev. Lett.* **125**, 154502 (2020).
- [26] P. Urban, P. Hanzelka, T. Králík, V. Musilová, and L. Skrbek, Thermal Waves and Heat Transfer Efficiency Enhancement in Harmonically Modulated Turbulent Thermal Convection, *Phys. Rev. Lett.* **128**, 134502 (2022).
- [27] R. Ostilla-Mónico, Y. Yang, E. P. van der Poel, D. Lohse, and R. Verzicco, A multiple-resolution strategy for direct numerical simulation of scalar turbulence, *J. Comput. Phys.* **301**, 308 (2015).
- [28] E. A. Fadlun, R. Verzicco, P. Orlandi, and J. Mohd-Yusof, Combined immersed-boundary finite-difference methods for three-dimensional complex flow simulations, *J. Comput. Phys.* **161**, 35 (2000).
- [29] See Supplemental Material at <http://link.aps.org/supplemental/10.1103/PhysRevLett.130.204001> for the details of numerical method and settings, the discussions about the dissipation rates, the effects of surface area, and the energy consumption.